MSDE

PAPER

View Article Online
View Journal | View Issue

Cite this: *Mol. Syst. Des. Eng.*, 2022, 7, 1045

Substituent effects on the mechanochemical response of zinc dialkyldithiophosphate†

Jie Zhang, James P. Ewen * and Hugh A. Spikes*

Mechanochemistry is known to play a key role in the function of some lubricant additives, such as the tribofilm growth of zinc dialkyldithiophosphate (ZDDP). This raises the intriguing possibility of tailoring the mechanochemical response of additives by modifying their alkyl substituents. Here, we study the tribofilm formation rate of ZDDPs containing several different alkyl groups on steel surfaces from a high-friction base oil. We use macroscale tribometer experiments under full-film elastohydrodynamic lubrication conditions to enable careful control of the temperature and stress during tribofilm growth. We show how the chain length and the presence of branches or bulky cycloaliphatic groups can lead to large differences in the temperature- and stress-dependencies of the tribofilm formation rate, which can be explained through variations in packing density, steric hindrance, and stress transmission efficiency. Our rate data are successfully fitted using the Bell model; a simple modification of the Arrhenius equation that is commonly employed to model the kinetics of mechanochemical processes. Using this model, we observe large differences in the activation energy, pre-exponential factor, and activation volume for the various ZDDPs. Our findings show how structure–performance relationships can be identified for lubricant additives, which may be useful to optimise their molecular structure.

Received 25th March 2022,
Accepted 27th May 2022

DOI: 10.1039/d2me00049k

rsc.li/molecular-engineering

Design, System, Application

Lubricant additives that reduce wear by forming protective tribofilms on rubbing surfaces are crucial to maintaining the efficient and reliable operation of many engineering systems. The most important of these additives is ZDDP, which has been used commercially for almost a century and remains ubiquitous in engine oils. While changes to the molecular structure of ZDDP are known to affect both its tribofilm formation and antiwear performance, the underlying physicochemical mechanisms are not well understood. This is partly due to the poorly defined temperature and stress conditions in standard tribometer experiments. Here, using carefully designed tribometer experiments under well-controlled conditions, we show how the mechanochemical reactivity of ZDDP can be altered by tailoring the additive's alkyl substituents. Specific examples include the observations that additives with long alkyl chains only form tribofilms at high temperature, while those containing bulky cycloaliphatic groups are particularly effective at high stress. We expect these findings to be useful for the rational design of high-performance lubricant additives for specific applications.

Introduction

The development of more sustainable lubricants with tailored tribological performance is a crucial activity in the pursuit of net zero greenhouse gas emissions.[1] Modern lubricants consist of a mixture of base oils (generally nonpolar hydrocarbons) that are blended with several different types of additives, which can be polar organic molecules, polymers, or organometallic compounds.[2] Probably the most important of these additives is zinc dialkyldithiophosphate (ZDDP), which was originally developed as an antioxidant, but is now used primarily for its remarkable antiwear performance.[3] ZDDP reduces wear by forming protective 'tribofilms' on rubbing steel surfaces.[3] Despite decades of research and development to find a more environmentally-friendly alternative,[4] ZDDP remains ubiquitous in engine lubricants. To rationally design antiwear additives with improved performance, a molecular-level understanding of the tribofilm formation and wear-reduction mechanisms of ZDDP is first required.[2] The tribofilms formed by ZDDP on steel substrates are mainly composed of zinc and iron polyphosphates.[3] These are formed by nucleophilic substitution reactions at the P atoms, which result in the formation of the P–O–P chains.[5] These reactions are dramatically accelerated once some of the alkyl or aryl groups

Department of Mechanical Engineering, Imperial College London, South Kensington Campus, London SW7 2AZ, UK. E-mail: j.ewen@imperial.ac.uk, h.spikes@imperial.ac.uk

† Electronic supplementary information (ESI) available: Information regarding the fluid film thickness calculations and friction measurements. Additional figures showing: a schematic of the ETM-SLIM setup, a comparison of SLIM images in different base oils, additional tribofilm growth measurements, bar charts to visualize the Bell model parameters for the various ZDDPs, and a plot comparing the rates measured experimentally to those predicted from the Bell model. See DOI: **https://doi.org/10.1039/d2me00049k**

(that are required to ensure the solubility of ZDDP in the base oil) are removed.[6] Therefore, ZDDPs containing different alkyl and aryl groups show greatly varying tribofilm growth and antiwear performance;[7–9] however, the underlying molecular mechanisms for these differences in macroscale behavior remain unclear.

In recent years, the mechanochemical aspects of ZDDP tribofilm formation have attracted widespread attention. Atomic force microscopy (AFM) experiments showed that ZDDP tribofilm formation rate increases exponentially with temperature and stress.[10] This discovery indicated that ZDDP tribofilm formation is a stress-augmented, thermally activated (SATA) process.[11] The rate constant, k, for a SATA process can be given by a modified form of the Arrhenius equation, which was originally proposed by Evans and Polanyi,[12] but is now usually known as the Bell model:[13]

$$k = A\exp\left(-\frac{E_a - \sigma\Delta V^*}{k_B T}\right) \quad (1)$$

where A is the pre-exponential factor, E_a is the activation energy, σ is the applied stress, ΔV^* is the activation volume, and k_B is the Boltzmann constant.[14] Although both the normal stress[10] and the shear stress[15,16] have been used in this equation for ZDDP tribofilm formation, recent experiments have demonstrated that the latter controls the reaction rate in macroscale experiments.[15,16] Tribometer experiments at different scales have suggested that ZDDP tribofilm formation follows either fractional-order[10,17] or zero-order[10,16] kinetics, indicating that ZDDP adsorbs onto steel surfaces before it dissociates and forms a tribofilm.

Much faster tribofilm growth has been observed for ZDDPs with secondary alkyl substituents compared to primary ones in macroscale tribometer experiments under both mixed/boundary (load mostly supported by the solid asperities)[8] and full-film elastohydrodynamic lubrication (EHL) (load supported by the pressurized lubricating fluid)[16] conditions. This has been rationalised by the greater stability of the carbocation formed during C–O cleavage (or C–S cleavage following alkyl group transfer)[3] in the former.[18] Since the initial cleavage reaction is probably the rate-determining step for ZDDP tribofilm formation,[16] the C–O (or C–S) bond is likely to be the key mechanophore for this process. Although shear stress controls the rate of tribofilm formation at the macroscale,[16] at the molecular level it is likely that the rate of cleavage is accelerated by the tensile component of this stress.[13] Experiments and first principles calculations have shown that stress can also affect the mechanical properties of ZDDP tribofilms once they have been formed.[19–21]

The structure and position of the chemical groups surrounding the mechanophore is known to influence the reactivity of mechanochemical processes. For example, in polymer mechanochemistry, longer chains are known to lead to enhanced reactivity in both bulk liquid flows[22] and solid grinding experiments.[23] Single-molecule force spectroscopy (SMFS) experiments have shown how a 'lever-arm effect' can enhance mechanochemical reactivity *via* polymer backbones acting as phenomenological levers that impose greater mechanical distortion on the mechanophore.[24] Cyclopropane-based polymers containing *E*-alkenes showed activation lengths (force-dependent equivalent of the stress-dependent activation volume) that were a third larger than those containing *Z*-alkenes.[25] Substituent effects can differ depending on the reaction pathway; for example, cyclobutene-based polymers containing *trans*-alkyl handles provided more mechanical leverage than *trans*-ester handles in conrotatory reactions, whereas *cis*-ester handles gave more mechanical leverage than *cis*-alkyl handles in disrotatory reactions.[26] The enhanced mechanical leverage of dialkyl relative to diester attachments was consistent with first principles calculations reported previously on *trans*-cyclobutene derivatives.[27] In similar polymers, replacing a methylene in the pulling attachment with a phenyl group dropped the applied force necessary to achieve a given rate constant in SMFS experiments by a factor of three, which was attributed to a combination of electronic stabilization and mechanical leverage effects.[28] More conventional substituent effects that can be explained through linear free energy relationships[29] have also been identified using SMFS. For example, spiropyran-derived polymers containing more electron-withdrawing substituents in the *para* position to the labile spirocyclic C–O bond required less force to break.[30] Substituent effects have also been predicted to affect the mechanochemical responses of small organic molecules from first principles calculations;[31,32] however, to our knowledge, substituent effects such as the lever arm effect are yet to be detected experimentally for organic or organometallic systems, such as ZDDP.

Here, we investigate the mechanochemical tribofilm formation of ZDDPs containing several different aliphatic substituents on steel surfaces in a ball-on-disk tribometer under full-film EHL conditions. The methods used here are similar to those described by Zhang *et al.*,[16] but employing different base oils and additives. In these experiments where there is negligible solid–solid contact, the temperature and shear stress conditions can be carefully controlled,[33] which is not the case in mixed/boundary lubrication conditions as present in most tribometers and mechanochemistry apparatus, such as ball mills.[34] This is because the stress is applied through confined base oil molecules rather than randomly contacting solid asperities.[15,16] This approach also avoids tribofilm wear[35] and other potential drivers of tribofilm growth, such as frictional heating, triboemission, and generation of catalytic surfaces.[36] For measurable tribofilm formation to occur under these conditions, large stresses are needed, which can be achieved by using either hard surfaces[15] or very high applied loads.[16] Moreover, base oils that provide high shear stress such as traction fluids with bulky cycloaliphatic groups[15,16] or polymers with pendant methyl groups[16] are required. High additive-surface affinity is also needed to form ZDDP tribofilms under these conditions.[37] Unlike previous studies using lower-purity

commercial additives,[10,15–17] the ZDDPs used here contain a wide range of well-defined alkyl groups to provide a more detailed understanding of the substituent effects on tribofilm growth under mechanochemical conditions. Using the Bell model,[13] large differences in the activation energy, pre-exponential factor, and activation volume for the various ZDDPs studied become apparent. We anticipate that these results will be useful both for the development of high-performance antiwear additives for specific applications[2] and for improving the accuracy of macroscale tribology models that include the effects of tribofilm growth.[38–41]

Methodology

Materials

All the tribometer experiments used through-hardened AISI 52100 steel balls and disks from PCS Instruments (Acton, UK). For the Hertz pressure and shear stress calculations,[16] the elastic modulus was taken as 207 GPa and 0.3 was used for the Poisson's ratio.[42] The ball had a root-mean-square (RMS) roughness, R_q = 8.5 nm, while for the disk, R_q = 6.0 nm. The steel ball and disc were soaked in toluene for at least 24 hours before a test and then ultrasonically cleaned in toluene, followed by Analar acetone, before being mounted in the tribometer.

We studied seven ZDDPs with different alkyl groups; four primary (oct-1-yl, 2-ethylhexyl, 2-cyclohexylethyl, and dodec-1-yl) and three secondary (oct-2-yl, but-2-yl, and 4-methylpent-2-yl). The ZDDPs were synthesized by Afton Chemical Corporation (Richmond, VA). ZDDP was first patented as a lubricant additive in the 1940s (ref. 3) and its synthesis has been reported numerous times in the literature.[43–45] The laboratory-prepared materials used here followed similar synthesis pathways, where the dithiophosphoric acid was prepared using P_2S_5 and the requisite alcohol, followed by reaction with ZnO to yield the desired ZDDP complex. The ZDDPs were synthesized from single high-purity (≥98%) alcohols, purchased from MilliporeSigma (St. Louis, MO) and used without further purification. This ensured that high-purity ZDDPs with well-defined chemical structures were tested.[9] Our ^{1}H-NMR and ^{13}C-NMR analysis confirmed that six of the ZDDPs contained only the expected alkyl group, while the oct-2-yl ZDDP contained 98 mol% oct-2-yl and 2 mol% oct-1-yl. Previous studies have suggested that negligible alkyl rearrangement occurs during ZDDP synthesis.[18] The ZDDPs were mostly (>80 mol%) in their neutral form, but they did contain a small amount of the basic form.[46] Previous tribology studies have shown that the two forms behave quite similarly.[3] All of the solutions contained a total ZDDP concentration of 800 ppm of phosphorus, which is similar to the treat rate used in commercial engine lubricant formulations.[16]

Strong additive adsorption is important to tribofilm formation under full-film EHL conditions.[37] Previous experiments have shown very similar adsorption behavior for linear primary (*n*-butyl), methyl-branched primary (i-butyl), and secondary (*s*-butyl) ZDDPs from *n*-hexadecane onto iron oxide powder.[47] Therefore, for most of the ZDDPs studied here, variation in the adsorption behavior is not expected to significantly affect the tribofilm formation rate on steel. However, for the ZDDPs containing longer branches[48] (2-ethylhexyl) and particularly the bulky cycloaliphatic substituents[49] (2-cyclohexylethyl), SAMs with lower packing densities are expected to form, which may affect their mechanochemical response.

Indopol H-8, provided by INEOS (London, UK), was used as the base oil for of the tribometer experiments in this study. This is a poly(butene) oligomer with an average molecular weight, M_n = 490 g mol^{-1} (degree of polymerisation ≈ 4) and a polydispersity index, M_w/M_n = 1.85. EHL fluid film thickness is determined by the lubricant viscosity at the inlet, where pressure is relatively low (~100 MPa). At ambient pressure, Indopol H-8 has a kinematic viscosity of 15 cSt at 100 °C, which is similar to the low-molecular weight poly(isobutene) (14 cSt at 100 °C), but is much higher than the base oil (6 cSt at 100 °C) poly(α-olefin) (PAO) and traction fluid (4 cSt at 100 °C) 2,3-dimethyl-2-[(3-methylbicyclo[2.2.1]hept-2-yl)methyl]-bicyclo[2.2.1]heptane (DM2H) that we have used previously.[16] The high viscosity of Indopol H-8 ensured that thick fluid EHL films (h > 50 nm) were formed under all of the conditions used here, resulting in negligible asperity contact.

The fluid film thickness of Indopol H-8 was measured in an EHD2 rig from PCS Instruments (Acton, UK) using ultra-thin film interferometry,[50] as shown in Fig. 1a. This technique requires the disk to be optically transparent, so a steel/glass contact, rather than steel/steel as used in the tribometer experiments, was employed. The measured fluid film thickness values were corrected using the equation due to Chittenden *et al.*[51] to account for the difference in reduced elastic modulus between glass and steel, as well as the large loads (W = 600–1500 N) applied in the subsequent tribofilm growth experiments (Table S1†). The severity of the asperity contact can be quantified by the λ ratio, which is the ratio of the EHL film thickness to the composite RMS surface roughness, R_{qc}. The R_{qc} of the steel/steel ball-on-disk combination was 10.4 nm, so the λ ratios in this study are between approximately 5 (120 °C) and 19 (60 °C). Since $\lambda \geq 5$, full-film EHL conditions with negligible direct asperity contact can therefore be assumed in all the tribofilm growth experiments.[52] This ensures that the stress conditions are well controlled[33] and also mitigates possible tribofilm wear[8] and competing tribochemical phenomena.[36]

Under mixed/boundary conditions, ZDDP tribofilms are considerably rougher than the underlying steel substrates.[53] If this were also to occur under full-film EHL conditions, lower λ ratios would be expected after prolonged rubbing than at the start of a tribofilm growth test, possibly leading to mixed rather than full-film EHL conditions. To assess this, the R_q of the tribofilms formed on the ball were estimated from the SLIM images (Table S2†). Note that these values are expected to be underestimated compared to independent

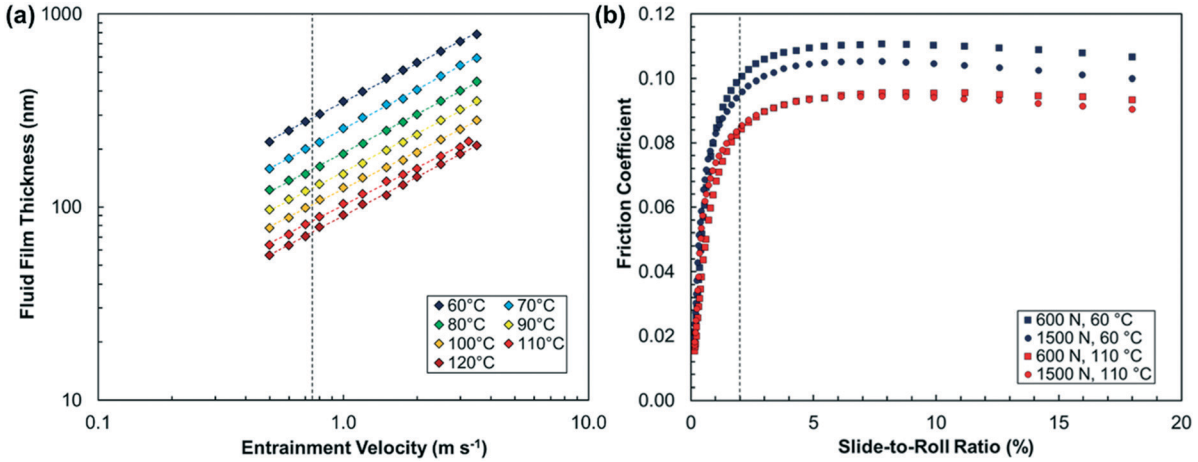

Fig. 1 (a) Variation in the fluid film thickness with entrainment velocity for Indopol H-8 at different temperatures (60–120 °C) and a constant load (20 N). The vertical black line indicates the entrainment velocity used in the tribofilm growth experiments (0.75 m s^{-1}). (b) Variation in the friction coefficient with SRR for Indopol H-8 at the different temperatures (60–110 °C) and loads (600–1500 N) used in the tribofilm growth experiments. The vertical black line indicates the SRR used in the tribofilm growth experiments (2%).

measurements obtained using AFM.[54] In general, the roughness of the tribofilms grown in the current study is similar to the underlying steel substrate. This is in agreement with previous comparisons using AFM,[16] where the tribofilms formed under full-film EHL conditions were found to be much smoother than those formed under mixed/boundary conditions. In general, the tribofilm roughness increases with tribofilm thickness and, in some cases, by the end of the test, the roughness of the tribofilm approaches the fluid film thickness ($\lambda \approx 1$). However, the tribofilm remains as smooth as the underlying steel substrate until its thickness exceeds 100 nm. Therefore, to calculate the growth rates, we only use the tribofilm thickness data up to approximately 100 nm, where full-film EHL conditions are maintained.

Unlike EHL film thickness, EHL friction is determined by viscosity in the central region of the contact, where the pressure is very high (>1 GPa).[33] Whereas lubricant base oils designed to give low friction such as PAO have low pressure–viscosity coefficients (α), some polymers (*e.g.* poly(isobutene)) and traction fluids (*e.g.* DM2H) have high α values.[16] Although the α value has not been reported for Indopol H-8, it is expected to be similar to the value measured for high-molecular weight poly(butenes) ($\alpha \approx 30$ GPa^{-1}).[55] Therefore, EHL friction (and thus shear stress) is likely to be sufficiently high to promote tribofilm growth on the steel surfaces in the accessible temperature and load range.[16] This was confirmed for the oct-1-yl ZDDP, which formed a tribofilm in tribometer experiments (Fig. S1†) under full-film EHL conditions at 1000 N and 80 °C from Indopol H-8, but not from PAO (Fig. S2†). Since both fluids are subjected to the same pressure, this observation reconfirms that the shear stress, rather than the normal stress, controls the mechanochemical response of ZDDP under full-film EHL conditions.[15,16] To quantify the shear stress conditions in the tribofilm growth experiments, we measured the friction coefficient in ball-on-disk tribometer experiments using the extreme-pressure traction machine (ETM) from PCS Instruments (Acton, UK). Fig. 1b shows that, in the absence of ZDDP, the friction coefficient of Indopol H-8 is high and slightly increases with increasing load and decreases with increasing temperature. The EHL friction was monitored throughout the tribofilm growth experiments (Table S3†) and it was observed that this quantity changed only slightly due to the presence of the ZDDP tribofilm.[16] To convert the measured EHL friction coefficients to maximum shear stresses, they were multiplied by the maximum Hertz pressure (P_{max} = 2.5–3.5 GPa) at the corresponding load (Table S4†). This approach provides the stress conditions in the central region of the ball-on-disk contact, where the tribofilm thickness is monitored.[16]

Methods

For the tribofilm growth measurements, we performed ball-on-disk tribometer experiments using the ETM (schematic shown in Fig. S1†).[16] We used the same ratio of the sliding velocity to the entrainment velocity, known as the slide-to-roll ratio (SRR = 2%) as in our previous tribofilm growth study.[16] Since Indopol H-8 has a higher viscosity than the traction fluid DM2H used in our previous study,[16] a sufficiently thick fluid film could be generated with a lower entrainment velocity (U = 0.75 m s^{-1}), and the sliding velocity was reduced accordingly (u_s = 0.015 m s^{-1}) to maintain the same SRR. This approach reduced frictional heating compared to the conditions used in our previous study.[16] The amount of frictional heating during the tribofilm growth experiments was estimated using the Archard equation,[56] employing the recently measured thermal conductivity of through-hardened AISI 52100 steel.[57] The rise in surface temperature in the contact due to frictional heating is expected to increase only slightly with load from 2.6 °C at 600 N to 4.8 °C at 1500 N. Thus, the significant increase in tribofilm formation rate at higher loads observed below cannot be explained by

frictional heating, which confirms mechanochemical acceleration.

During each test, the lubricant was added to the test chamber and the system was heated with the ball and disc rotating but not in contact. Once the desired lubricant temperature (T = 60–120 °C) was reached, a short running-in procedure was carried out at conditions of U = 0.1 m s^{-1}, SRR = 50%, and W = 100 N load for 1 minute. This stage neither resulted in any measurable change in surface roughness of the specimens nor was it essential for subsequent tribofilm formation; however, it did improve the repeatability of the tribofilm formation tests, possibly by removing any adsorbed contaminants on the test specimens by rubbing.[16] The contact was then unloaded and U increased to 0.75 m s^{-1} with SRR = 2%. The target load (W = 600–1500 N) was then applied and an extended test carried out under full-film EHL conditions. Unlike tribofilm growth experiments under mixed/boundary conditions,[8] there is no induction period at the start of the tests. The accessible loads yield a maximum Hertz pressure of 2.5–3.5 GPa and thus a maximum shear stress of 250–350 MPa in the steel/steel ball-on-disk contact.[16]

The tribofilm thickness was determined every 5–15 minutes using spacer-layer imaging (SLIM).[58] During the tests, the ball was raised from the disk, its rotational motion was halted, and it was loaded upward, within the test chamber, against a coated glass window with a load of 100 N. White light was then shone into the resulting stationary contact, where some is reflected by a semi-reflective coating on the underside of the glass. The remaining light passes through a silica spacer layer and the tribofilm formed on the ball, before being reflected back from the steel substrate. The two beams undergo optical interference depending on their optical path difference, which corresponds to the tribofilm thickness. An interference image was captured as a red-green-blue (RGB) pixel map using a high-resolution camera. A calibration chart of RGB colour *versus* optical path difference obtained using ultra-thin film interferometry[50] was then used to convert this RGB pixel map to a tribofilm thickness map. A refractive index of 1.6 was assumed for the tribofilm.[8] A representative set of SLIM images and the corresponding tribofilm thicknesses are shown in Fig. 2. The mean tribofilm thickness was taken over a circle of diameter 40 μm at the centre of the contact and the standard deviation was used to determine the composite RMS roughness, R_{qc}, of the tribofilms on the steel ball and disk (Table S2†). To calculate the growth rates, linear fits to the tribofilm thickness data up to approximately 100 nm (filled symbols in Fig. 2) are used.

Results and discussion

Fig. 3 shows how the tribofilm thickness varies with rubbing time for the different ZDDP solutions in Indopol-H8 at the same concentration (800 ppm P), temperature (80 °C) and load (1000 N) condition. At the start of the tests, the tribofilm formation rate is approximately linear in all cases, which is consistent with zero-order kinetics. Note that previous experiments with commercial ZDDPs found no concentration dependence on the tribofilm growth rate in the range 200–800 ppm P, thus confirming zero-order kinetics and the decomposition of adsorbed ZDDP molecules.[16] The tribofilm formation rates are much higher for all the secondary ZDDPs than the primary ones, which is consistent with previous tribometer experiments with commercial ZDDPs under mixed/boundary[8] and full-film EHL conditions.[16] The three secondary ZDDPs and one of the primary ZDDPs (oct-1-yl) level out at a maximum tribofilm thickness of between 50–150 nm, while the other primary ZDDPs continue to increase linearly over the duration of the experiments. A similar range

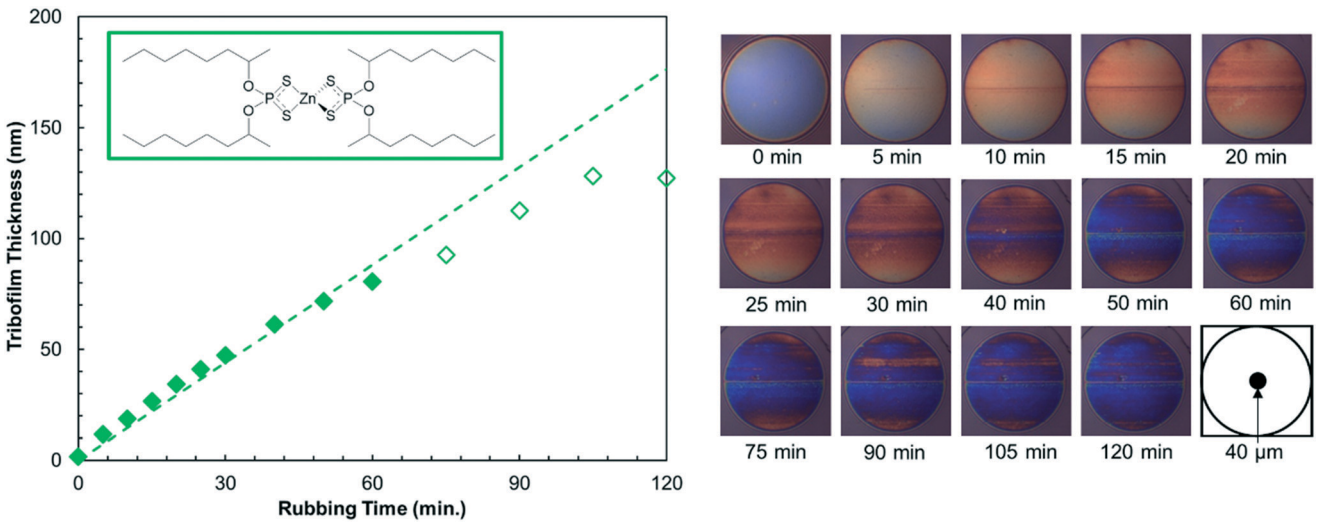

Fig. 2 Representative example (oct-2-yl ZDDP at 80 °C and 1000 N) of the tribofilm thickness growth over time, measured from the SLIM images shown on the right. Dashed linear fits are used to calculate the growth rates (filled symbols only). Black circle (diameter = 40 μm) represents the area over which the mean tribofilm thickness was measured in the central region of the contact.

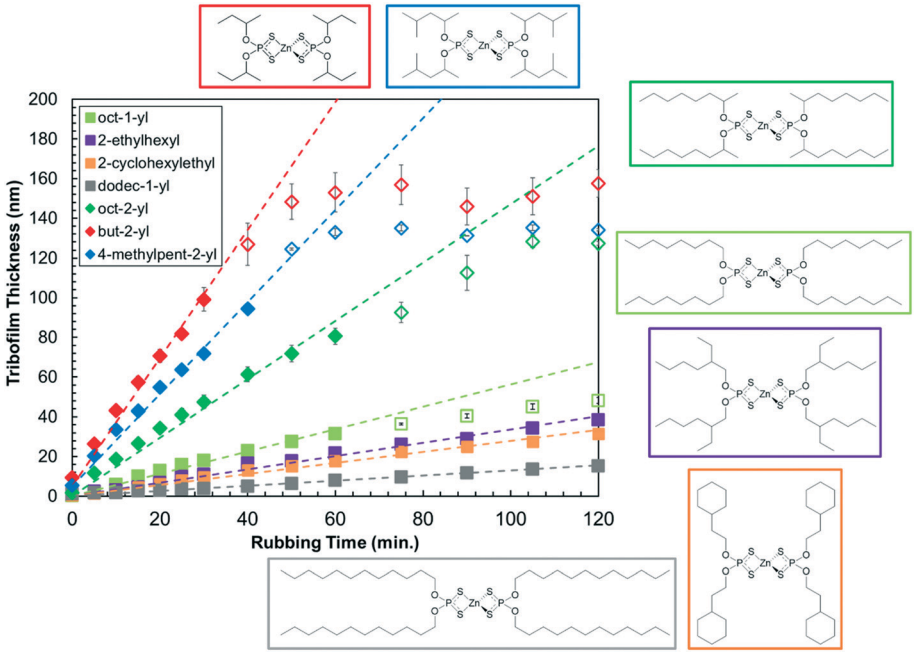

Fig. 3 Variation in the tribofilm thickness with rubbing time for the primary (oct-1-yl, 2-ethylhexyl, 2-cyclohexylethyl, and dodec-1-yl) and secondary (oct-2-yl, but-2-yl, and 4-methylpent-2-yl) ZDDPs for a single temperature (80 °C) and load (1000 N) condition in steel/steel contacts. Points represent mean results from three tests and vertical bars represent one standard deviation. Dashed linear fits are used to calculate the growth rates (filled symbols only).

of maximum tribofilm thicknesses have been observed in previous experiments.[8,10,16] This levelling-off behavior has been attributed to the reduction in contact stress for thicker ZDDP tribofilms due to their lower stiffness compared to the underlying steel substrate.[10]

The differences in tribofilm formation rate with chain length, branching, and the presence of cycloaliphatic groups are more subtle. For the primary alkyl ZDDPs, the tribofilm growth rate at 80 °C and load 1000 N increases in the order: dodec-1-yl < 2-cyclohexylethyl < 2-ethylhexyl < oct-1-yl. Comparing the linear alkyls, the ZDDP with the longer chains (dodec-1-yl) forms tribofilms much more slowly than the one with shorter chains (oct-1-yl). A reduction in friction with increasing chain length has also been reported for oct-1-yl and dodec-1-yl ZDDPs under boundary lubrication conditions.[59] These observations suggest that ZDDP (or its dissociation products) form self-assembled monolayers (SAMs) on top of the growing ZDDP tribofilm that are responsible for both the boundary friction response[9] and surface reactivity. SAM formation has also been linked to the antiwear performance of ZDDPs in previous studies where molecules with larger monolayer cohesive energies gave lower wear.[60,61] It has been shown for a range of systems and processes at solid–liquid interfaces, that SAMs formed from surfactants with longer alkyl chains generally show lower chemical reactivity.[62–64] This is due to the formation of more densely packed, ordered monolayers[65] that are more difficult for approaching molecules to penetrate to react with the surface. This effect is likely responsible for the slower tribofilm growth of dodec-1-yl ZDDP than octyl-1-yl ZDDP, since the more densely packed monolayer hinders further adsorption, decomposition, and ultimately tribofilm formation on the steel surface. For the primary ZDDPs with C_8 alkyl groups, the tribofilm growth rate increases in the order: 2-cyclohexylethyl < 2-ethylhexyl < oct-1-yl. This suggests that the increased steric bulk has a larger effect on the rate than the lower packing density expected for the ethyl-branched[48] and particularly cyclohexyl-containing[49] ZDDPs compared to the linear one. Previous studies of other systems have also shown lower reactivity for surfaces protected by branched alkyl monolayers compared to linear ones.[48,66]

For the secondary alkyl ZDDPs at 80 °C and 1000 N, the reactivity increases in the order: oct-2-yl < 4-methylpent-2-yl < but-2-yl. The trend is similar to the primary ZDDPs in that the secondary ZDDPs with longer alkyl chains give slower tribofilm formation rates, which can again be attributed to the formation of more densely packed SAMs. The presence of methyl branches in the 4-methylpent-2-yl ZDDP seems to have a minimal effect on the tribofilm growth rate, since the rate is approximately halfway between oct-2-yl and but-2-yl, as would be expected for a linear hex-2-yl group. A similar order of tribofilm growth rate for ZDDPs with the same substituents has recently been reported under mixed/boundary conditions,[9] where the tribofilm will be partially worn away as it grows.[8]

To obtain a more complete understanding of substituent effects on mechanochemical reactivity of ZDDP, we studied how the tribofilm formation rate varied with temperature (60–120 °C) and load (600–1500 N). Fig. 4 shows the tribofilm growth for a representative primary (oct-1-yl) and secondary

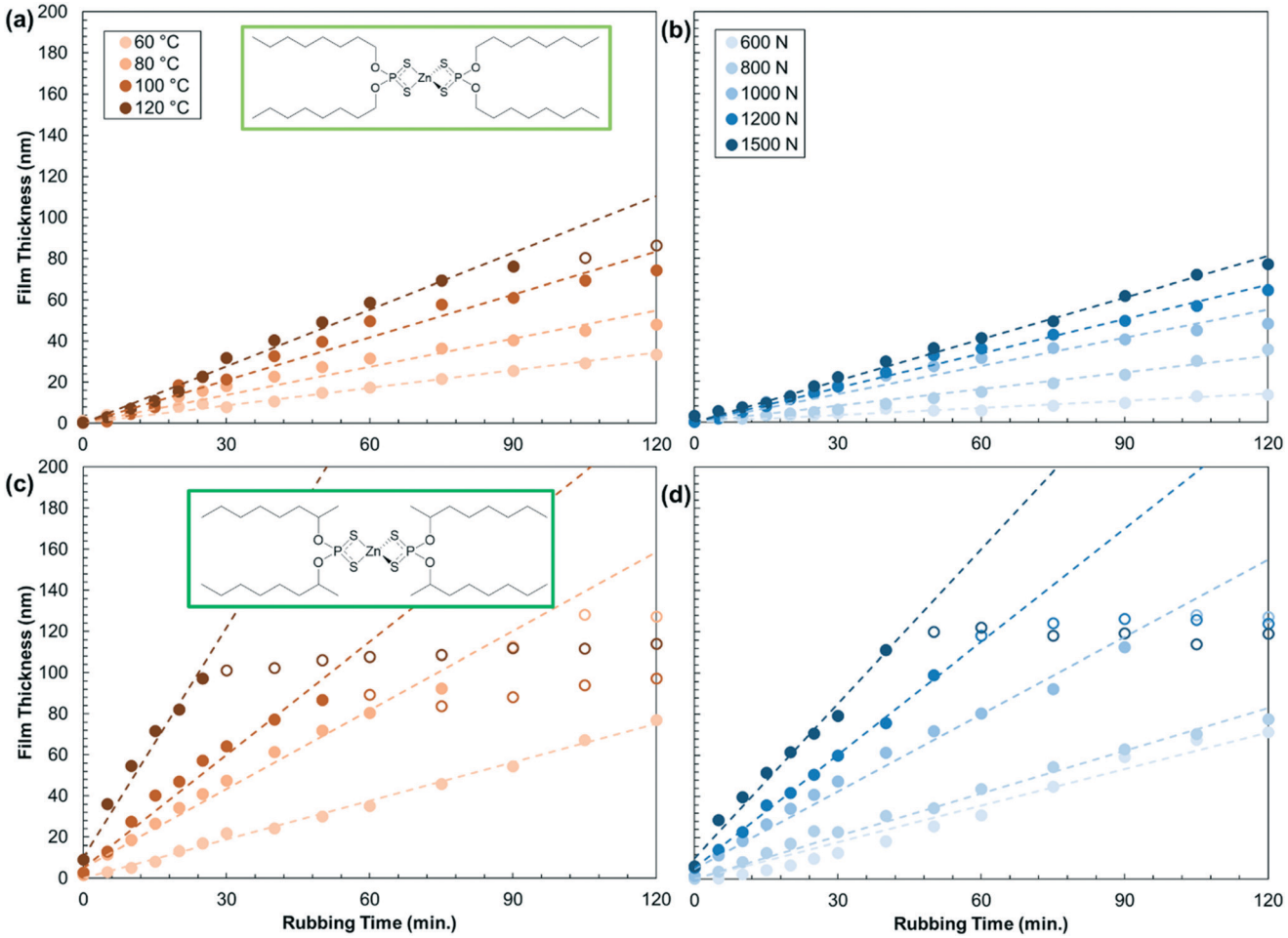

Fig. 4 Variation in the tribofilm formation rate with temperature at a constant load of 1000 N (a and c) and shear stress at a constant temperature of 80 °C (b and d) for primary oct-1-yl (a and b) and secondary oct-2-yl (c and d) ZDDPs. Results for the other ZDDPs are shown in the Fig. S3 and S4.† Dashed linear fits are used to calculate the growth rates (filled symbols only).

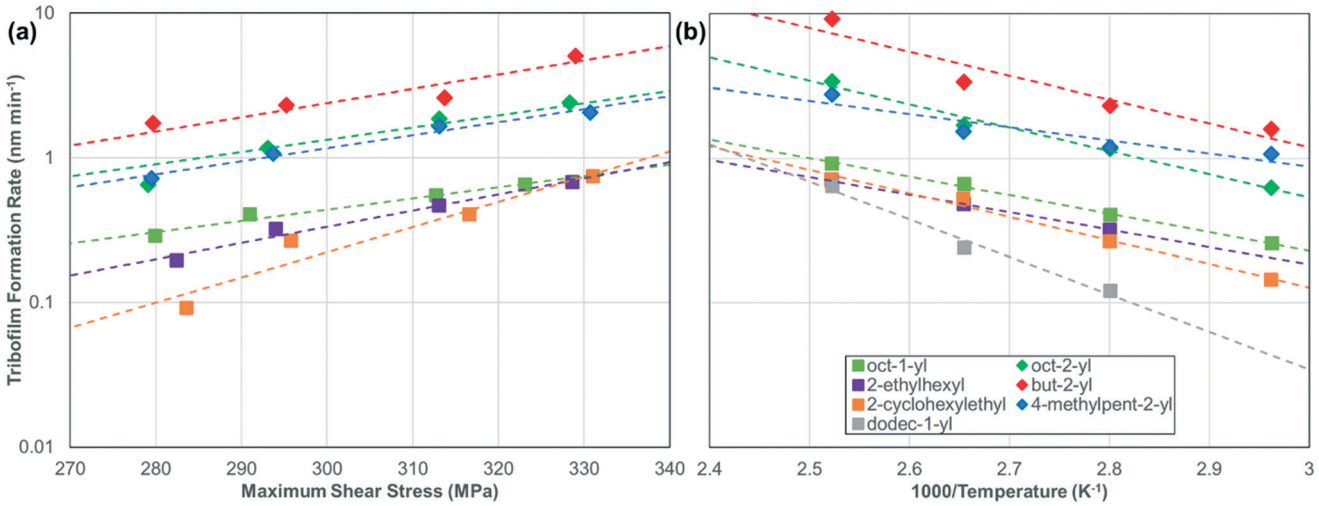

Fig. 5 Change in the tribofilm growth rate for the various ZDDPs with (a) maximum shear stress, τ_{max}, at 80 °C and (b) inverse temperature, 1000/T, at 1000 N (P_{max} = 3 GPa). Dashed lines are exponential fits of the data to eqn (1).[13] The rate *versus* shear stress data for the oct-1-yl and dodec-1-yl ZDDPs at 120 °C are shown in Fig. S5.†

(oct-2-yl) ZDDP. Initially, the tribofilm thickness increases linearly for both ZDDPs before it asymptotes towards a constant thickness. The growth rate and maximum film thickness both increase with temperature and load. The growth rate is faster for the oct-2-yl ZDDP than the oct-1-yl ZDDP for all the temperature-load combinations studied. Results for the other primary and secondary ZDDPs are shown in Fig. S3 and S4,† respectively.

Fig. 5 shows the temperature and shear stress dependence of the tribofilm growth rate for all the ZDDPs. The rates (Table S5†) are calculated from the slopes of the linear fits in Fig. 4, S3, and S4.† For all the ZDDPs, the growth rate increases exponentially with both temperature and shear stress, which is indicative of a SATA process.[11] Under all the conditions studied, the tribofilm growth rate is much faster for the secondary ZDDPs than the primary ZDDPs.[16] The tribofilm growth rate is negligible ($<$0.1 nm min^{-1}) for the dodec-1-yl ZDDP when $T < 80$ °C, irrespective of the load. This could be due to the formation of a close-packed SAM by the dodec-1-yl ZDDP at low temperature that becomes less ordered (or possibly partially desorbed) at higher temperature, allowing additional ZDDP molecules to adsorb, decompose, and form tribofilms. For dodec-1-yl thiol SAMs on gold surfaces, the order–disorder transition temperature is 50 °C,[65] while the desorption temperature is 110 °C.[67] The headgroup–substrate affinity will affect these values, so it is not possible to determine whether an order–disorder transition or desorption is the primary cause of the substantial increase in reactivity of the dodec-1-yl ZDDP above 80 °C. From an application-focused perspective, this type of antiwear additive might be useful in high-temperature applications (such as heavy-duty diesel engines[68]) because it would effectively form tribofilms and also provide very low boundary friction under these conditions.[9]

Using eqn (1) (Bell model),[13] the slopes of the rate *versus* stress (Fig. 5a) plots were used to calculate ΔV^*, while the slopes and intercepts of the rate *versus* temperature (Fig. 5b) plots were used to calculate E_a and ln(A), respectively (see Table 1 and Fig. S6†).[69] The shear stress, rather than the normal stress, was used in eqn (1) since previous studies have shown that the former controls the tribofilm formation rate under full-film EHL conditions.[15,16] The ΔV^* values are also normalized by the molecular volumes, V_{mol} shown in Table 1 that were calculated using the 3 V software with a probe size of 3 Å^3.[70] The ZDDP structures used were relaxed in ChemBio3D Ultra 14 Suite (PerkinElmer, Waltham, MA) using the MM2 force field.[71]

At 80 °C, the ΔV^* is slightly smaller for the primary oct-1-yl (0.09 nm^3) ZDDP than the secondary oct-2-yl (0.10 nm^3) ZDDP, implying a similar stress-dependency of their reactivity. The E_a is higher for the oct-2-yl (66 kJ mol^{-1}) than the oct-1-yl (56 kJ mol^{-1}) ZDDP, despite the lower thermal stability of secondary ZDDPs.[5,72] These E_a values are consistent with previous measurements for commercial secondary (82 kJ mol^{-1}),[16] primary (56 kJ mol^{-1}),[16] and mixed primary/secondary (79 kJ mol^{-1})[10] ZDDPs. On the other hand, A is around two orders of magnitude larger for the oct-2-yl (2.5×10^5 nm s^{-1}) than the oct-1-yl (5.9×10^3 nm s^{-1}) ZDDP. Since the difference in E_a suggests faster rates for oct-1-yl than oct-2-yl, the experimentally observed larger rates for oct-2-yl must be due to the differences in ΔV^* and particularly A. This can be visualized in Fig. 5, where the rates for the oct-2-yl ZDDP are shifted vertically (larger intercept) with respect to the oct-1-yl ZDDP. These observations are also consistent with the differences noted by Zhang *et al.*,[16] although the differences in A between the commercial secondary (2.0×10^7 nm s^{-1}) and primary (1.1×10^3 nm s^{-1}) were even larger than in the current study. The current experiments support the hypothesis that the mechanochemical decomposition of primary and secondary ZDDPs proceeds through different chemical mechanisms.[16] While previous glassware experiments in the absence of steel surfaces have suggested a common mechanism for thermal decomposition of ZDDP,[5] first principles calculations have shown that the C–O bonds are broken through different mechanisms for primary and secondary ZDDPs; alkyl group transfer (from –OR to –SR) for the former and alkene elimination for the latter.[73]

The $\Delta V^*/V_{mol}$ values in Table 1 suggest that a 7–17% deformation of the ZDDP molecules occurs when moving from the ground state to the transition state for the mechanochemical reaction.[74] These values fall within the range estimated for other tribological processes involving molecular systems (2–27%), which have been derived both from experiments and molecular simulations.[14,69,75–78] The ΔV^* values are also similar to those obtained previously for commercial primary (0.13 nm^3) and secondary (0.15 nm^3) ZDDPs.[16] Comparing the values for oct-1-yl at 80 °C (0.09 nm^3) and 120 °C (0.14 nm^3), there is an increase in ΔV^* with

Table 1 Kinetic parameters extracted from the fits to eqn (1) shown in Fig. 5. Mean values are shown with 95% confidence intervals. E_a and A calculated at 1000 N, most ΔV^* calculated at 80 °C (* some ΔV^* calculated at 120 °C)

Substituent	E_a kJ mol^{-1}	A nm s^{-1}	ln(A)	ΔV^* nm^3	V_{mol} nm^3	$\Delta V^*/V_{mol}$%
Oct-1-yl	56 ± 1	5.9×10^3	9 ± 1	0.09 ± 0.01	1.26	7 ± 1
	74 ± 1*	1.2×10^5*	12 ± 1*	0.14 ± 0.01*		11 ± 1*
2-Ethylhexyl	68 ± 2	1.9×10^4	10 ± 1	0.13 ± 0.01	1.32	10 ± 1
2-Cyclohexylethyl	102 ± 3	2.1×10^7	17 ± 1	0.20 ± 0.04	1.18	17 ± 3
Dodec-1-yl	123 ± 9*	1.8×10^{10}*	24 ± 3*	0.19 ± 0.02*	1.72	11 ± 1*
Oct-2-yl	66 ± 4	2.5×10^5	12 ± 1	0.10 ± 0.02	1.18	9 ± 2
But-2-yl	72 ± 7	1.7×10^6	14 ± 3	0.11 ± 0.02	0.78	14 ± 3
4-Methylpent-2-yl	55 ± 6	4.4×10^3	8 ± 2	0.10 ± 0.02	1.03	9 ± 2

increasing temperature. This observation is consistent with recent NEMD simulations.[69] Recent first principles calculations of hydroxylated silica–silica interfaces showed that ΔV^* is inversely proportional to the contact stiffness. However, this effect cannot fully explain the large (40%) increase in ΔV^* observed here between 80 °C and 120 °C, because the elastic modulus of AISI 52100 steel is expected to drop by less than 10% over this temperature range.[42] There do not seem to be any systematic differences between the ΔV^* values for primary and secondary ZDDPs. However, comparing the ΔV^* values of the oct-1-yl (0.14 nm^3) and dodec-1-yl (0.19 nm^3) ZDDPs at 120 °C, there is a clear increase in this parameter with increasing chain length. Moreover, at 80 °C, the primary C_8 ZDDPs containing branched (2-ethylhexyl, 0.13 nm^3) and particularly the bulky cycloaliphatic (2-cyclohexylethyl, 0.20 nm^3) substituents have larger ΔV^* values than those with linear (oct-1-yl, 0.09 nm^3) alkyl groups. The exact physicochemical meaning of ΔV^* remains unclear for tribochemical reactions;[79,80] however, a larger activation volume (or activation length[24,25]) implies that, at a given stress, there is a greater distortion of the molecule from the ground state to the transition state along the reaction path.[74] In other words, compared to the oct-1-yl groups, the longer dodec-1-yl, branched 2-ethylhexyl and particularly bulky 2-cyclohexylethyl groups act as metaphorical crowbars, allowing the shear (or tensile[13]) stress to be transmitted across a greater distance as the initial C–O (or C–S) bond-breaking reaction proceeds.[28] This implies that the lever-arm effect, previously identified in polymer mechanochemistry using SMFS under applied tensile force,[24] can also affect mechanochemical reactivity of comparatively small organometallic compounds such as ZDDP under applied shear stress. From a practical perspective, ZDDPs with branched and cycloaliphatic substituents might be particularly useful for wear protection in low-temperature, high-stress applications, such as gear oils.[81]

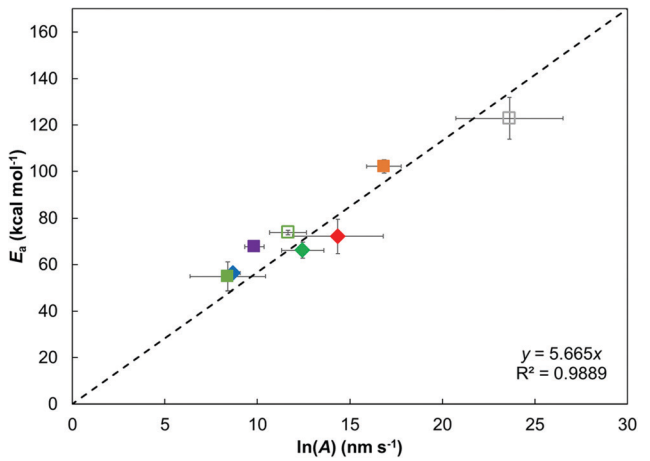

Fig. 6 Linear relation between E_a and ln(A) for the different ZDDPs studied, suggesting a kinetic compensation effect.[82] Vertical and horizontal bars show 95% confidence intervals. Legend is the same as in Fig. 5, closed symbols use ΔV^* calculated at 80 °C, open symbols at 120 °C.

Fig. 6 shows that, for the various ZDDPs studied here, there is a linear relationship between E_a and ln(A), which is indicative of the kinetic compensation effect.[82] ZDDPs that have a large E_a also show higher ln(A) (*e.g.* dodec-1-yl), which suggests both a high energy barrier and a high frequency of successful collisions.[12] From transition state theory,[74] this can also be interpreted as the tribofilm growth reactions having a larger enthalpic barrier, but also a smaller entropic penalty.[82] ZDDPs with primary linear alkyl groups sit on the linear fit in Fig. 6 (within statistical uncertainty), while those with branched (2-ethylhexyl) and cycloaliphatic (2-ethylcylohexyl) primary alkyl groups sit above it. Thus, ZDDPs with branched and cycloaliphatic groups have a larger E_a for a given ln(A) compared to ZDDPs with linear alkyl groups, which can be attributed to their higher thermal stability due to increased steric bulk. Conversely, most of the ZDDPs with secondary alkyl groups (oct-2-yl and but-2-yl) fall below the linear fit in Fig. 6, implying a smaller E_a for a given ln(A), which can be attributed to their lower thermal stability, due to the increased stability of the secondary carbocation formed during their dissociation.[5,18,72]

In this study, we have demonstrated that the Bell model[13] can be used to explain the large differences in mechanochemical reactivity of ZDDPs with various alkyl substituents (Fig. S7†). Linear secondary alkyl ZDDPs are inherently less stable than primary ones with the same chain length under mechanochemical conditions, which is mostly due to a higher pre-exponential factor (Table 1).[16,69] Since they form SAMs with a higher packing density,[9] ZDDPs with longer alkyl chain lengths require higher temperatures to form tribofilms, which manifests as a higher activation energy. The activation volume increases with alkyl chain length and when moving from linear, to branched, and to cycloaliphatic substituents. These trends can be rationalised through a molecular-scale analogue of the lever-arm effect that has consistenly been observed in polymer mechanochemistry.[24] These kinetic parameters can be used directly to inform macroscale tribology models that consider tribofilm growth inside rubbing contacts.[38–41] We also expect that, coupled with information regarding their friction and wear performance under mixed/boundary conditions,[9] the improved understanding of substituents effects on tribofilm growth identified here under mechanochemical conditions will be useful in the rational design of antiwear additives with improved performance for specific applications such as lubricants for heavy-duty diesel engines[68] and gear oils.[81] More generally, the methods proposed here can be used to identify molecular structure–performance relationships for lubricant additives under well-controlled conditions, as recently achieved for viscosity modifier additives[83] and synthetic base oils.[84]

Conclusions

We have studied the tribofilm formation rate of four primary and three secondary ZDDPs with well-defined alkyl

substituents in steel/steel contacts under full-film EHL conditions. For all the ZDDPs, the tribofilm growth rate increases exponentially with temperature and shear stress, which confirms that this is a SATA process. We observe large differences in the temperature- and shear stress-dependencies of the various ZDDPs. We have shown how the parameters for the Bell equation can be used to rationalise the order of mechanochemical reactivity for the different ZDDPs. Our results suggest that the chain length, branching and presence of bulky cycloaliphatic groups in the ZDDP alkyl substituents may affect the packing density, steric hindrance, and stress transmission, and result in significant differences in the activation energy, pre-exponential factor, and activation volume. These parameters can be used directly for the development of more accurate macroscale tribology models that consider the effect of growing of tribofilms. We also anticipate that these findings will be useful for the rational design of high-performance lubricant additives for specific applications.

Conflicts of interest

There are no conflicts to declare.

Acknowledgements

We thank the Engineering and Physical Sciences Research Council (EPSRC) for funding *via* grant EP/P030211/1. J. Z. thanks Shell for funding through the Shell-Imperial University Technology Centre for Fuels & Lubricants. J. P. E. was supported by the Royal Academy of Engineering through the Research Fellowships scheme. We thank PCS Instruments Ltd. for provision of the ETM tribometer, INEOS Group Ltd. for the supply of base oils, and Afton Chemical Corp. for the supply of ZDDP additives. We are grateful to Keith Hayes (Afton Chemical) for the ZDDP synthesis. We thank Carlos Ayestarán Latorre (Imperial College London), Joseph E. Remias (Afton Chemical) and W. T. Tysoe (University of Wisconsin-Milwaukee) for useful discussions.

References

1 S. Liu, T. R. Josephson, A. Athaley, Q. P. Chen, A. Norton, M. Ierapetritou, J. I. Siepmann, B. Saha and D. G. Vlachos, *Sci. Adv.*, 2019, **5**, eaav5487.
2 R. I. Taylor, *Faraday Discuss.*, 2012, **156**, 361–382.
3 H. Spikes, *Tribol. Lett.*, 2004, **17**, 469–489.
4 H. Spikes, *Lubr. Sci.*, 2008, **20**, 103–136.
5 R. B. Jones and R. C. Coy, *ASLE Trans.*, 1981, **24**, 91–97.
6 N. J. Mosey and T. K. Woo, *Inorg. Chem.*, 2006, **45**, 389–395.
7 J. F. Graham, C. McCague and P. R. Norton, *Tribol. Lett.*, 1999, **6**, 149–157.
8 H. Fujita and H. A. Spikes, *Proc. Inst. Mech. Eng., Part J*, 2004, **218**, 265–277.
9 J. Zhang, M. Ueda, S. Campen and H. Spikes, *Tribol. Lett.*, 2021, **69**, 8.
10 N. N. Gosvami, J. A. Bares, F. Mangolini, A. R. Konicek, D. G. Yablon and R. W. Carpick, *Science*, 2015, **348**, 102–106.
11 H. A. Spikes, *Friction*, 2018, **6**, 1–31.
12 M. G. Evans and M. Polanyi, *Trans. Faraday Soc.*, 1935, **31**, 875–894.
13 G. I. Bell, *Science*, 1978, **200**, 618–627.
14 A. Boscoboinik, D. Olson, H. Adams, N. Hopper and W. T. Tysoe, *Chem. Commun.*, 2020, **56**, 7730.
15 J. Zhang and H. Spikes, *Tribol. Lett.*, 2016, **63**, 24.
16 J. Zhang, J. P. Ewen, M. Ueda, J. S. S. Wong and H. A. Spikes, *ACS Appl. Mater. Interfaces*, 2020, **12**, 6662–6676.
17 A. Dorgham, P. Parsaeian, A. Azam, C. Wang, A. Morina and A. Neville, *Tribol. Int.*, 2019, **133**, 288–296.
18 W. W. Hanneman and R. S. Porter, *J. Org. Chem.*, 1964, **29**, 2996–2998.
19 N. J. Mosey, M. H. Müser and T. K. Woo, *Science*, 2005, **307**, 1612–1615.
20 D. Shakhvorostov, M. H. Müser, N. J. Mosey, Y. Song and P. R. Norton, *Phys. Rev. B: Condens. Matter Mater. Phys.*, 2009, **79**, 094107.
21 S. V. Sukhomlinov and M. H. Müser, *Tribol. Lett.*, 2021, **69**, 89.
22 J. A. Odell and A. Keller, *J. Polym. Sci., Part B: Polym. Phys.*, 1986, **24**, 1889–1916.
23 H. Oka, K. Imato, T. Sato, T. Ohishi, R. Goseki and H. Otsuka, *ACS Macro Lett.*, 2016, **5**, 1124–1127.
24 H. M. Klukovich, T. B. Kouznetsova, Z. S. Kean, J. M. Lenhardt and S. L. Craig, *Nat. Chem.*, 2013, **5**, 110–114.
25 J. Wang, T. B. Kouznetsova, Z. S. Kean, L. Fan, B. D. Mar, T. J. Martínez and S. L. Craig, *J. Am. Chem. Soc.*, 2014, **136**, 15162–15165.
26 C. L. Brown, B. H. Bowser, J. Meisner, T. B. Kouznetsova, S. Seritan, T. J. Martinez and S. L. Craig, *J. Am. Chem. Soc.*, 2021, **143**, 3846–3855.
27 Y. Tian and R. Boulatov, *ChemPhysChem*, 2012, **13**, 2277–2281.
28 B. H. Bowser, S. Wang, T. B. Kouznetsova, H. K. Beech, B. D. Olsen, M. Rubinstein and S. L. Craig, *J. Am. Chem. Soc.*, 2021, **143**, 5269–5276.
29 P. R. Wells, *Chem. Rev.*, 1963, **63**, 171–219.
30 M. H. Barbee, T. Kouznetsova, S. L. Barrett, G. R. Gossweiler, Y. Lin, S. K. Rastogi, W. J. Brittain and S. L. Craig, *J. Am. Chem. Soc.*, 2018, **140**, 12746–12750.
31 M. Krupička and D. Marx, *J. Chem. Theory Comput.*, 2015, **11**, 841–846.
32 M. Á. Fernández-González and L. M. Frutos, *J. Chem. Phys.*, 2021, **154**, 224106.
33 H. Spikes and Z. Jie, *Tribol. Lett.*, 2014, **56**, 1–25.
34 K. Uzarevic, I. Halasz and T. Frisic, *J. Phys. Chem. Lett.*, 2015, **6**, 4129–4140.
35 M. Ueda, A. Kadiric and H. A. Spikes, *Tribol. Lett.*, 2019, **67**, 123.
36 T. E. Fischer, *Annu. Rev. Mater. Sci.*, 1988, **18**, 303–323.
37 M. Ueda, A. Kadiric and H. Spikes, *Tribol. Online*, 2020, **15**, 318–331.
38 A. Ghanbarzadeh, P. Parsaeian, A. Morina, M. C. T. Wilson, M. C. P. van Eijk, I. Nedelcu, D. Dowson and A. Neville, *Tribol. Lett.*, 2016, **61**, 12.

39 A. Akchurin and R. Bosman, *Tribol. Lett.*, 2017, **65**, 59.
40 Z. Chen, C. Gu and T. Tian, *Tribol. Lett.*, 2021, **69**, 13.
41 J. Yang, W. Pu and X. Pei, *Surf. Topogr.: Metrol. Prop.*, 2021, **9**, 025017.
42 Y. B. Guo and C. R. Liu, *J. Manuf. Sci. Eng.*, 2002, **124**, 1–9.
43 V. P. Wystrach, E. O. Hook and G. L. M. Christopher, *J. Org. Chem.*, 1956, **21**, 705–707.
44 E. S. Yamaguchi, P. R. Ryason and E. Q. Labrador, *Tribol. Trans.*, 1995, **38**, 243–250.
45 E. S. Yamaguchi, P. R. Ryason, E. Q. Labrador and T. P. Hansen, *Tribol. Trans.*, 1996, **39**, 220–224.
46 S. Menzer, J. R. Phillips, A. M. Z. Slawin, D. J. Williams and J. D. Woollins, *J. Chem. Soc., Dalton Trans.*, 2000, 3269–3273.
47 S. Plaza, *ASLE Trans.*, 1987, **30**, 233–240.
48 O. Elimelech, O. Aviv, M. Oded, X. Peng, D. Harries and U. Banin, *ACS Nano*, 2022, **16**, 4308–4321.
49 S. Kwon, Y. Choi, J. Choi, H. Kang, H. Chung and J. Noh, *Ultramicroscopy*, 2008, **108**, 1311–1314.
50 R. Gohar and A. Cameron, *Nature*, 1963, **200**, 458–459.
51 R. J. Chittenden, D. Dowson, J. F. Dunn and C. M. Taylor, *Proc. R. Soc. London, Ser. A*, 1985, **397**, 245–269.
52 C. R. Evans and K. L. Johnson, *Proc. Inst. Mech. Eng., Part C*, 1987, **201**, 145–150.
53 L. Taylor, A. Dratva and H. A. Spikes, *Tribol. Trans.*, 2000, **43**, 469–479.
54 K. Topolovec-Miklozic, T. R. Forbus and H. A. Spikes, *Tribol. Lett.*, 2007, **26**, 161–171.
55 S. Bair, *J. Non-Newtonian Fluid Mech.*, 2001, **97**, 53–65.
56 J. F. Archard, *Wear*, 1959, **2**, 438–455.
57 T. Reddyhoff, A. Schmidt and H. Spikes, *Tribol. Lett.*, 2019, **67**, 22.
58 P. M. Cann, H. A. Spikes and J. Hutchinson, *Tribol. Trans.*, 1996, **39**, 915–921.
59 S. Aoki, A. Suzuki and M. Masuko, *Proc. Inst. Mech. Eng., Part J*, 2006, **220**, 343–351.
60 S. Y. Jiang, R. Frazier, E. S. Yamaguchi, M. Blanco, S. Dasgupta, Y. H. Zhou, T. Cagin, Y. C. Tang and W. A. Goddard III, *J. Phys. Chem. B*, 1997, **101**, 7702–7709.
61 Y. H. Zhou, S. Y. Jiang, T. Cagin, E. S. Yamaguchi, R. Frazier, A. Ho, Y. C. Tang and W. A. Goddard III, *J. Phys. Chem. A*, 2000, **104**, 2508–2524.
62 F. P. Zamborini and R. M. Crooks, *Langmuir*, 1998, **14**, 3279–3286.
63 A. C. Templeton, M. J. Hostetler, C. T. Kraft and R. W. Murray, *J. Am. Chem. Soc.*, 1998, **120**, 1906–1911.
64 B. Dordi, H. Schönherr and G. J. Vancso, *Langmuir*, 2003, **19**, 5780–5786.
65 P. Fenter, P. Eisenberger and K. S. Liang, *Phys. Rev. Lett.*, 1993, **70**, 2447–2450.
66 X. Bin, T. K. Mischki, C. Fan, G. P. Lopinski and D. D. M. Wayner, *J. Phys. Chem. C*, 2007, **111**, 13547–13553.
67 U. H. Pi, J. H. Kim, H. Y. Yu, C. W. Park, S. Y. Choi, Y. K. Kim and J. S. Ha, *Surf. Sci.*, 2006, **600**, 625–631.
68 D. Pierce, A. Haynes, J. Hughes, R. Graves, P. Maziasz, G. Muralidharan, A. Shyam, B. Wang, R. England and C. Daniel, *Prog. Mater. Sci.*, 2019, **103**, 109–179.
69 C. Ayestarán Latorre, J. E. Remias, J. D. Moore, H. A. Spikes, D. Dini and J. P. Ewen, *Commun. Chem.*, 2021, **4**, 178.
70 N. R. Voss and M. Gerstein, *Nucleic Acids Res.*, 2010, **38**, 555–562.
71 N. L. Allinger, *J. Am. Chem. Soc.*, 1977, **99**, 8127–8134.
72 J. J. Dickert and C. N. Rowe, *J. Org. Chem.*, 1967, **32**, 647–653.
73 N. J. Mosey and T. K. Woo, *J. Phys. Chem. A*, 2004, **108**, 6001–6016.
74 H. Eyring, *J. Chem. Phys.*, 1935, **3**, 107.
75 J. Yeon, X. He, A. Martini and S. H. Kim, *ACS Appl. Mater. Interfaces*, 2017, **9**, 3142–3148.
76 X. He and S. H. Kim, *Langmuir*, 2017, **33**, 2717–2724.
77 A. Khajeh, X. He, J. Yeon, S. H. Kim and A. Martini, *Langmuir*, 2018, **34**, 5971–5977.
78 X. Chen, K. Kawai, H. Zhang, K. Fukuzawa, N. Koga, S. Itoh and N. Azuma, *J. Phys. Chem. C*, 2020, **124**, 22496–22505.
79 Z. Li and I. Szlufarska, *Phys. Rev. Lett.*, 2021, **126**, 076001.
80 A. Martini and S. H. Kim, *Tribol. Lett.*, 2021, **69**, 150.
81 A. Adebogun, R. Hudson, A. Matthews and P. J. Withers, *Tribol. Lett.*, 2020, **68**, 48.
82 E. Roduner, *Chem. Soc. Rev.*, 2014, **43**, 8226–8239.
83 L. Cosimbescu, D. Malhotra, K. B. Campbell, M. S. Swita and Z. C. Kennedy, *Mol. Syst. Des. Eng.*, 2019, **4**, 1114–1124.
84 J. Y. Xue, S. Q. Dong, P. K. Mi, L. B. Wang, S. H. Wang, Z. Zhang, Z. G. Zhang and J. S. Hu, *Mol. Syst. Des. Eng.*, 2021, **6**, 722–729.